

Article

Structure and Properties of Al–0.6 wt.%Zr Wire Alloy Manufactured by Direct Drawing of Electromagnetically Cast Wire Rod

Nikolay Belov ^{1,2,*}, Maxim Murashkin ^{3,4}, Natalia Korotkova ¹, Torgom Akopyan ^{1,2} 
and Victor Timofeev ⁵

¹ Department of Metal Forming, National University of Science and Technology MISiS, Leninsky prospekt 4, Moscow 119049, Russia; kruglova.natalie@gmail.com (N.K.); nemiroffandtor@yandex.ru (T.A.)

² Laboratory for Gradient Materials, Nosov Magnitogorsk State Technical University, Lenin pr., 38, Magnitogorsk 455000, Russia

³ Institute of Physics of Advanced Materials, Ufa State Aviation Technical University, K. Marx 12, Ufa 450008, Russia; m.murashkin.70@gmail.com

⁴ Laboratory for Mechanics of Bulk Nanostructured Materials, St. Petersburg State University, Universitetskaya nab. 7/9, St. Petersburg 199034, Russia

⁵ Department of Electrical Engineering, Siberian Federal University, 79 Svobodnyy Prospekt, Krasnoyarsk 660041, Russia; viktortim0807@mail.ru

* Correspondence: nikolay-belov@yandex.ru; Tel.: +79-154-145-945

Received: 5 May 2020; Accepted: 6 June 2020; Published: 9 June 2020



Abstract: The method of electromagnetic casting (EMC) was used to produce the long-length rod billet (with a diameter 12 mm) of aluminum alloy containing 0.6 wt.% Zr, 0.4%Fe, and 0.4%Si. The combination of high cooling rate ($\approx 10^4$ K/s) during alloy solidification and high temperature before casting (≈ 830 °C) caused zirconium to dissolve almost completely in the aluminum solid solution (Al). Additions of iron and silicon were completed in the uniformly distributed eutectic $\text{Al}_8\text{Fe}_2\text{Si}$ phase particles with an average size of less than 1 μm . Such fine microstructure of the experimental alloy in as-cast state provides excellent deformability during wire production using direct cold drawing of EMC rod (94% reduction). TEM study of structure evolution in the as-drawn 3 mm wire revealed the onset of Al_3Zr (L_{12}) nanoparticle formation at 300 °C and almost-complete decomposition of (Al) at 400 °C. The distribution of Zr-containing nanoparticles is quite homogeneous, with their average size not exceeding 10 nm. Experimental wire alloy had the ultimate tensile strength (UTS) and electrical conductivity (EC) (234 MPa and 55.6 IACS, respectively) meeting the AT2 type specification. At the same time, the maximum heating temperature was much higher (400 versus 230 °C) and meets the AT4 type specification.

Keywords: aluminum-zirconium wire alloys; electromagnetic casting; drawing; electrical conductivity; phase composition; nanoparticles

1. Introduction

Aluminum alloys containing the addition of zirconium (0.2–0.4 wt.%) are widely used for manufacturing of heat resistant wires. Such alloys possess the improved combination of electrical conductivity, mechanical properties, and, particularly, thermal stability [1–3]. The most common commercial technology for wire rods production (including Al–Zr alloys) is the technology of continuous casting and rolling (CCR) realized in Properzi and Southwire rolling mills [4,5]. To meet the American Society for Testing and Materials (ASTM) specification (AT1–AT4 types) for the heat resistance [1], the microstructure should have a sufficient amount of Zr-containing precipitates (of metastable phase

Al₃Zr having L1₂ crystal lattice) [6]. These precipitates should have a size within 10 nm and uniform distribution. To obtain such nanoparticles, zirconium should be fully dissolved in the aluminum solid solution (hereinafter (Al)) during solidification. Nanoparticles of Al₃Zr phase form during decomposition of the supersaturated aluminum solid solution (hereinafter (Al)) [7–11]. At the same time, to meet the ASTM specification for electrical conductivity, the concentration of Zr in (Al) should be as minimal as possible. The microstructure of Al–Zr wire alloy depends considerably on the processing route, particularly melting and casting temperatures and parameters of annealing [6,12,13]. As a rule, the CCR wire rods are subjected to annealing at temperatures above 350 °C during a long time of holding. Moreover, complete (Al) decomposition and formation of a sufficient number of L1₂ nanoparticles requires holding CCR wire rods for hundreds of hours.

As shown earlier [14], electromagnetic casting (EMC) provides sufficiently high casting temperatures and ultra-high solidification rates (10³–10⁴ K/s) and allows the production of long rod billets with a diameter of 8–12 mm. This rapid solidification in the EMC method corresponds to the solidification of granules, which is realized in the RS/PM (rapid solidification/powder metallurgy) method [15,16]. This method has been most successfully applied to obtain alloys with a high content of transition metals, including zirconium. Recently, it was shown that for the experimental Al–0.6Zr–0.4Fe–0.4Si (wt.%) alloy in the form of a long 8 mm diameter ingot that the EMC method was very suitable for wire alloys with increased content of zirconium [17]. The technological route used in this work included operations of rolling and intermediate annealing. Based on these results, the aim of this work was to study the structure and properties of the aluminum wire alloy containing 0.6%Zr, obtained using direct cold drawing from an as-cast 12 mm diameter EMC rod.

2. Experimental Methods

The experimental alloy in form of the long rod billets with a diameter of 12 mm and ≈20 m in length was obtained by EMC using equipment of the Research and Production Centre of Magnetic Hydrodynamics (Krasnoyarsk, Russia) [18]. This equipment consisted of an induction furnace, magnetic hydrodynamic (MHD)-stirrer, dosing trough, and electromagnetic crystallizer. Coolant from a cooling reservoir was supplied to the workpiece directly, which provides high cooling speed. The alloy was smelted in a graphite-chased crucible from commercial aluminum (99.5 wt.%) and master alloys (containing zirconium, iron, and silicon) at ≈850 °C. The temperature of melt before casting (≈830 °C) was higher than the liquidus temperature (822 °C).

The wire (3 mm diameter) was manufactured from the as-cast EMC rod on a dragging mill (the reduction ratio was 94%). This wire was studied in as-drawn state and after annealing at 300–400 °C (Figure 1). To estimate the effect of deformation on the decomposition of (Al) during annealing, a 2 mm strip was made additionally from the as-cast EMC billet by cold rolling. This strip was annealed together with the EMC rod at 300–600 °C. The annealing modes used are summarized in Table 1. It should be noted that the annealing modes used were previously substantiated in [6] for the Al alloys, which hardened due to the nanoparticles of the L1₂ phase. Values for the Vickers hardness and electrical resistivity (ER) were measured at each regime.

The microstructure was examined by means of scanning electron microscopy (SEM, TESCAN VEGA 3, Tescan Orsay Holding, Brno, Czech Republic), electron microprobe analysis (EMPA, OXFORD Aztec, Oxford Instruments, Oxfordshire, UK), and transmission electron microscopy (TEM, JEM 2100, JEOL, Tokyo, Japan), at an accelerating voltage of 200 kV. To study the microstructure, thin foils were used, produced by jet polishing on a Tenupol-5 machine (Struers, Ballerupcity, Denmark) with the chemical solution consisting of 20% nitric acid and 80% methanol at a temperature of –25 °C and a voltage of 15 V. The SEM specimens were electrolytically polished at 12 V in an electrolyte containing six parts C₂H₅OH, one part HClO₄, and one part glycerin.

The Vickers hardness (HV) was measured using a DUROLINE MH-6 universal tester (METKON Instruments Inc., Bursa, Turkey), with a load of 1 kg and a dwell time of 10 s. The hardness was measured at least five times at each point. The specific electrical conductivity (EC) of the EMC rod and

the cold rolled strip was determined using the eddy current method with a VE-26NP eddy structures cope (CJSC Research institute of introscopy SPEKTR, Moscow, Russia). The electrical resistivity (ER) of the EMC rod and the strip was calculated from the EC data. The electrical resistivity of the cold drawn wire was measured in accordance with IEC 60468:1974 standard [19] for straightened samples of at least 1 m in length in the rectified part.

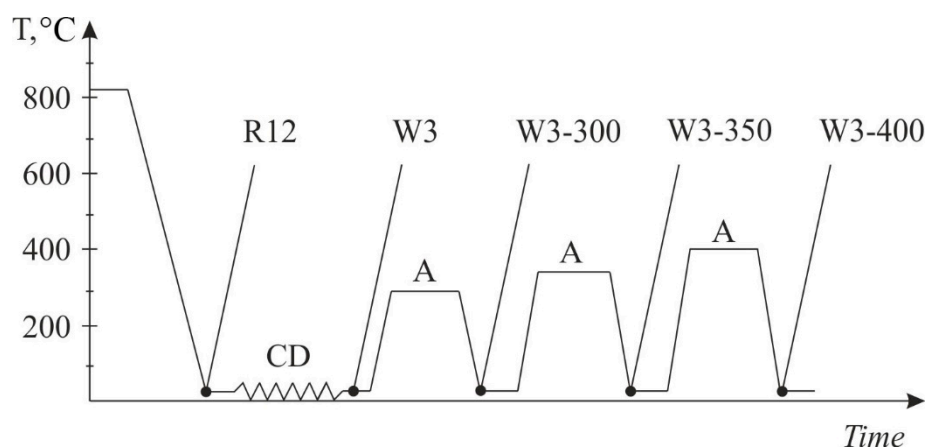


Figure 1. Processing root for experimental wire alloy (see Table 1). CD—cold drawing, A—annealing, R12—as-cast electromagnetic casting (EMC) rod, and W3—wire.

Table 1. Annealing regimes for EMC rod, strip and wire.

Designation	Regime Treatment
R12-EMC casting rod (diameter 12 mm)/S2-cold rolled strip (thickness 2 mm)	
R12/S2	As-cast/as-cold rolled
R12-300/S2-300	Annealing at 300 °C, 3 h
R12-350/S2-350	R12-300/S2-300 + annealing at 350 °C, 3 h
R12-400/S2-400	R12-350/S2-350 + annealing at 400 °C, 3 h
R12-450/S2-450	R12-400/S2-400 + annealing at 450 °C, 3 h
R12-500/S2-500	R12-450/S2-450 + annealing at 500 °C, 3 h
R12-550/S2-550	R12-500/S2-500 + annealing at 550 °C, 3 h
R12-600/S2-600	R12-550/S2-550 + annealing at 600 °C, 3 h
W-Wire (diameter 3 mm) manufactured by cold drawing of as-cast EMC rod	
W3	As-drawn
W3-300	Annealing at 300 °C, 3 h
W3-350	W300 + annealing at 350 °C, 3 h
W3-400	W350 + annealing at 400 °C, 3 h

The as-processed wire specimens were tensile tested at room temperature on a Zwick Z250 (ZwickRoell AG, Ulm, Germany) universal testing machine at a loading rate of 10 mm/min. Yield strength (YS), ultimate tensile strength (UTS), and elongation to failure (El.) were determined. To obtain consistent results, five specimens were tested.

The size of the dendritic cells was experimentally determined using metallography from high-contrast microstructural images processed with appropriate software, Sizer (National University of Science and Technology MISiS, Moscow, Russia). The Horizontal Lines option was used for implementing the stereological method of measuring the relative length of the phase regions. To obtain reliable data, we analyzed at least 10 fields in the microstructure to define the content of each structural component. The experimental dendritic cell size data were used for evaluating the cooling rate in the alloy crystallization temperature range using a well-known function [20].

3. Results and Discussion

3.1. Characterization of as-Cast EMC Rod

Due to the high solidification rate of the as-cast ingot, the microstructure of the experimental alloy has a fine structure. Only a small quantity of primary Al_3Zr phase crystals were revealed (Figure 2a). According to EMPA, the concentration of zirconium in (Al) was very close to its total content in the alloy (0.58 versus 0.62%). The measured average size of the dendritic cells was $4.2 \pm 1.6 \mu\text{m}$ (Figure 2b), which, according to coefficients given in [20] for the technical grade aluminum 1050, corresponded to a cooling rate of about $2.5 \times 10^4 \text{ K/s}$. Iron-bearing particles in the form of thin veins were located along the boundaries of the dendritic cells. As shown earlier [17], these veins correspond to the $\text{Al}_8\text{Fe}_2\text{Si}$ phase. It should be noted that the microstructure was analyzed over the entire cross section of the ingot, and no significant differences were found between the structural parameters (as well as hardness values measured in different sections of the ingot). It can be assumed that a relatively small cross section (12 mm in diameter) and a high cooling rate during solidification provided the formation of a relatively uniform structure.

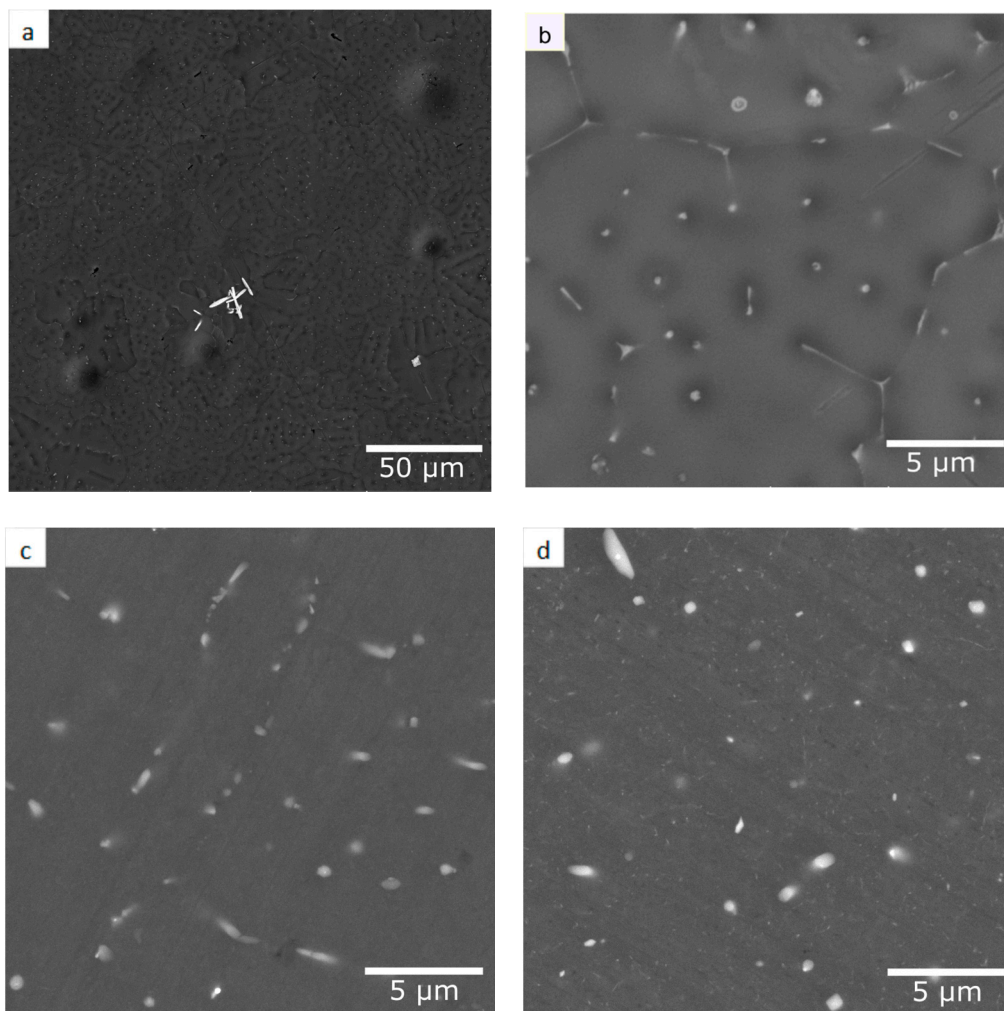


Figure 2. Effect of annealing temperature on microstructures of the EMC rod, SEM: (a,b) as-cast (R0), (c) 500 °C (R500), and (d) 600 °C (R600).

Annealing of the as-cast rod at up to 400 °C made no visible changes to its microstructure. The morphology of the $\text{Al}_8\text{Fe}_2\text{Si}$ phase changed at higher temperatures. Annealing at 450 °C produced spherical particles of this phase, which is preferable to most of the other iron bearing phases (particularly,

Al₃Fe and Al₅FeSi) that have a needle-shaped morphology [21–23]. Most of the veins transformed to globular particles upon annealing at 500 °C (Figure 2c). Increasing the annealing temperature leads to particle enlargement, and the maximum particle size in the R12-600 state (Table 1) reaches 1 µm (Figure 2d). In this state, the alloy also contains precipitates attributable to a stable Zr-bearing phase [8,24], i.e., Al₃Zr (D0₂₃). Calculations show [17] that these two phases should be in equilibrium with (Al) in this state.

3.2. Effect of Annealing on Hardness and Electrical Conductivity

Alloys containing at least 0.4%Zr are known to undergo substantial hardening during the precipitation of these particles [5]. The EMC rod hardness vs. final annealing stage temperature curve (Figure 3a) showed that the hardening was significant at 350 °C, reaching the highest level at 400 °C (the R12-400 state). Increasing the annealing temperature leads to a significant decrease in HV, which can be accounted for, primarily, by coarsening of the Al₃Zr precipitates [7–11]. The hardness of the cold rolled strip was higher compared to that of the EMC rod (650 vs. 400 MPa). Deformation hardening was retained upon strip annealing to 400 °C. Annealing at higher temperatures leads to a significant softening which can be attributed to the formation of recrystallized grains. In a range of 450–500 °C, the hardness of the EMC rod was much higher than that of the strip, but the difference decreased noticeably with an increase in the annealing temperature. After annealing at 600 °C, they had approximately the same hardness (67–70 HV), mainly because of the coarsening of the Al₃Zr precipitates (at this temperature they should transform completely to the equilibrium D0₂₃ phase) [25–28].

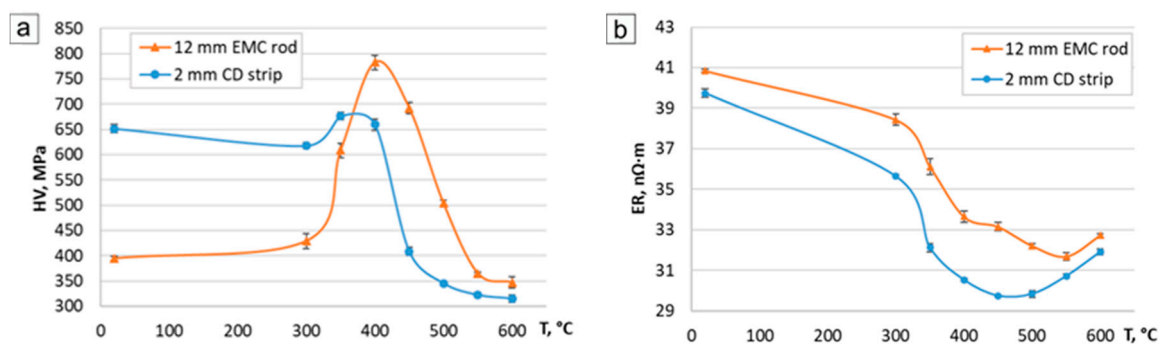


Figure 3. Hardness (HV) (a) and electrical resistivity (ER) (b) vs. temperature of annealing curves for EMC rod and cold rolled strip.

The formation of L1₂ (Al₃Zr) nanoparticles leads to a decrease in the Zr concentration in (Al) according Al–Zr phase diagram [6]. This process promotes the decrease of electrical resistivity [29,30], as shown in Figure 3b. The ER decreased from 40.8 to 31.2 nΩm for the EMC rod, and from 39.7 to 29.8 nΩm for the cold rolled strip. The decomposition rate of (Al) in the cold rolled strip is higher than that in the EMC rod. Indeed, in the former case, the minimum ER was reached after annealing at 450 °C, while in the latter case it was reached at 550 °C. In both cases, these temperatures are higher than the maximum hardening point (Figure 3a). The increase of ER at higher temperatures can be accounted for by an increase in the solubility of Zr in (Al) [6,27]. The non-recrystallized structure was preserved in strip after annealing at up to 400 °C (states S2-400). Since the best combination of hardness and ER in the cold rolled strip was reached after annealing at this temperature, we did not consider annealing the wire at higher temperatures.

3.3. Structure and Properties of Wire

We supposed the manufacturability of the as-cast EMC rod during drawing was very good. This was favored as its fine microstructure did not contain coarse intermetallic particles or inhomogeneities. Cold drawing led to the formation of elongated grains and deformation hardening. Drawing also crushed initial eutectic Al₈Fe₂Si phase veins into submicron globular particles (Figure 4a,b).

It was seen that high-temperature annealing (W400 mod) leads to coarsening of the particles (Figure 4b). Since the as-drawn state (W3 in Table 1) did not imply heating, (Al) retained all the zirconium, which dissolved in it during crystallization. Therefore, the ER for all the initial states (R12, S2 and W3) proved to be close (about 40 nΩm). Figure 5 shows that the ER of the wire and the strip are very close after annealing.

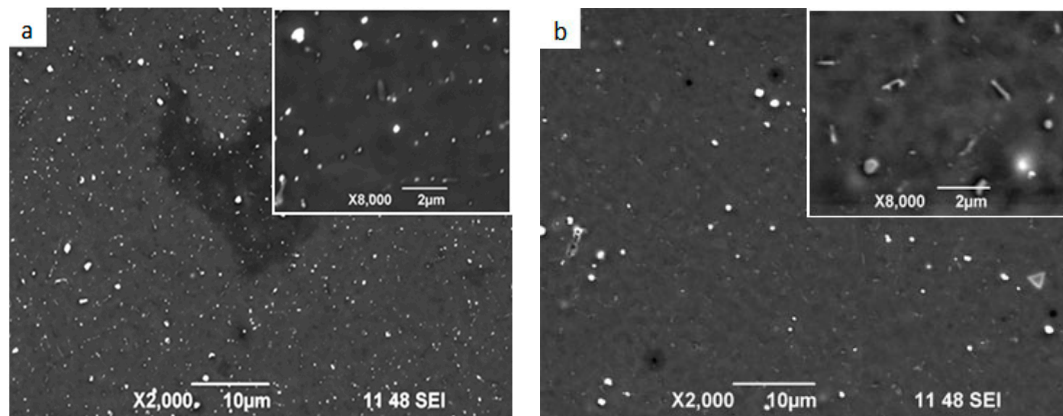


Figure 4. SEM structure of the 3 mm wire after cold drawing (from as-cast EMC rod) and annealing at 300 °C (W300, see in Table 1) (a) and 300 + 350 + 400 °C (W400 see in Table 1) (b).

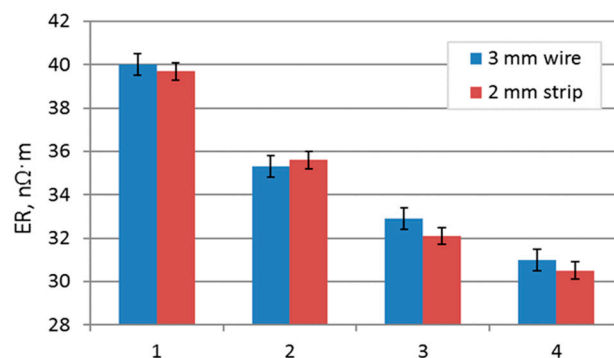


Figure 5. Comparison of electrical resistivity (ER) of 3mm wire and 2 mm strip for Al–0.6%Zr–0.4%Fe–0.4%Si alloy: 1—as-cast, 2—300 °C, 3—300 + 350 °C, 4—300 + 350 + 400 °C.

The structural changes caused by annealing were analyzed in detail using TEM. The structure annealed at 300 °C (state W300 in Table 1) contained (Al) grains and subgrains (Figure 6a), and showed the onset of Al₃Zr (L1₂) nanoparticles formation (Figure 6b,c). However, relatively large particles reaching ≈50 nm in size also precipitated at subgrain boundaries (Figure 6d). The presence of Fe- and Zr-bearing particles were confirmed by the direct energy-dispersive X-ray spectroscopy (EDX) analysis of their composition. According to ER data (see Figure 4), the decomposition of (Al) after annealing at 300 °C should be uncompleted. Thus, part of Zr should remain in (Al).

Annealing at 400 °C (state W400 in Table 1) largely changes the TEM structure because of the formation of multiple L1₂ nanoparticles inside subgrains (Figure 7b). The distribution of these nanoparticles were quite homogeneous, with their average size being within 10 nm. The reflections in the selected-area electron diffraction (SAED) patterns are much brighter (Figure 7c), as compared with those for the W300 state (Figure 6c). Taking into account the decrease of ER (Figure 3), one can conclude that (Al) decomposition after annealing at 400 °C was almost complete. This structure provides for the optimal combination of strength, electrical resistivity, and, particularly, thermal stability [31].

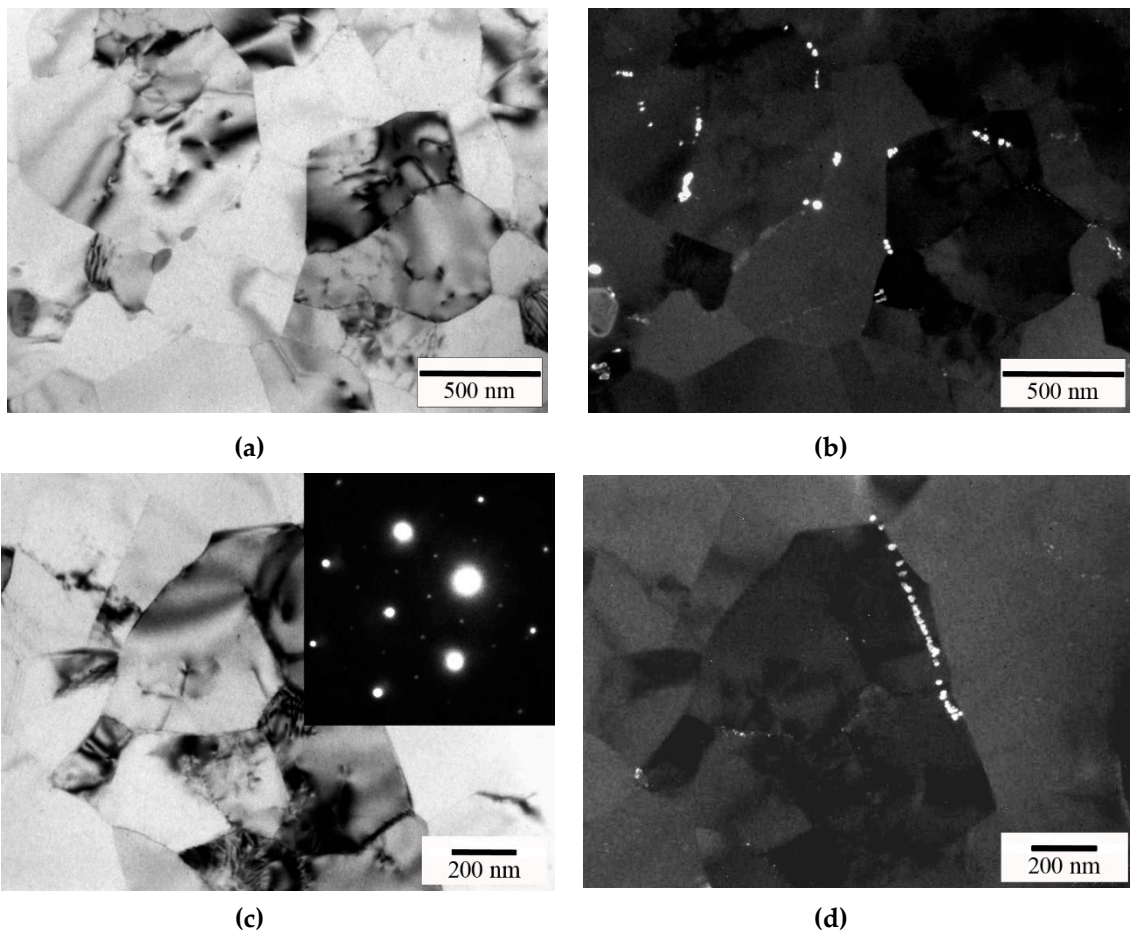


Figure 6. TEM image in the cross section of the experimental alloy after cold drawing and annealing at 300 °C (W300, see in Table 1): (a,c) bright field (BF); (b,d) dark field (DF); (c) BF TEM image and corresponding SAED patterns (the crystal is close to the [111] zone axis orientation) and (d) DF TEM image showing Al_3Zr phase nanoparticles present in the Al matrix.

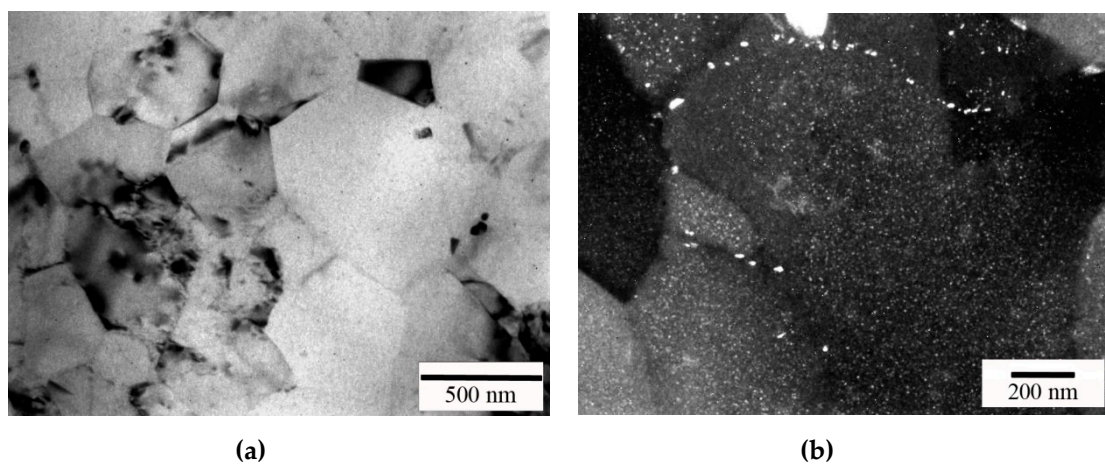


Figure 7. *Cont.*

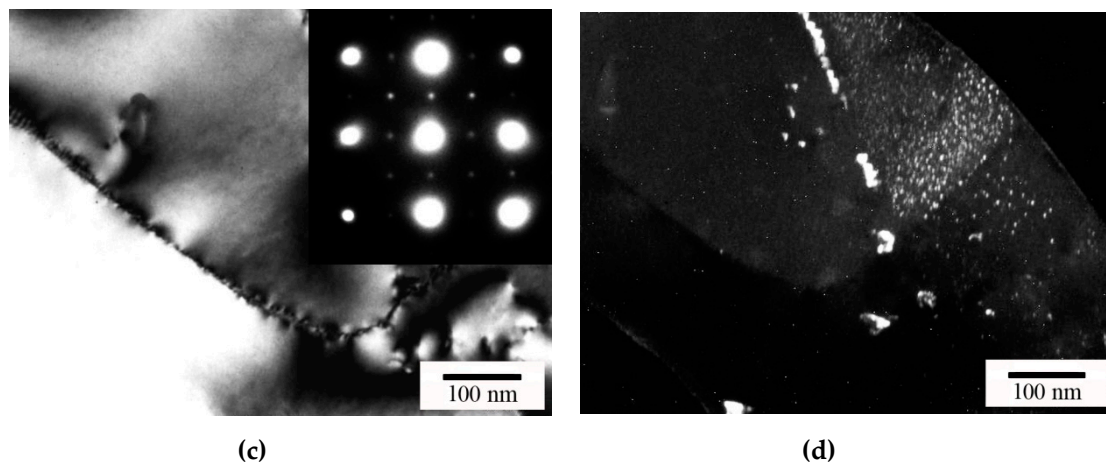


Figure 7. TEM image in the cross section of the Al alloy after cold drawing and annealing at 300 + 350 + 400 °C (W400 see in Table 1): (a,c) bright field (BF); (b,d) dark field (DF); (c) BF TEM image and corresponding SAED patterns (the crystal is close to the [001] zone axis orientation) and (d) DF TEM image showing Al_3Zr phase nanoparticles present in the Al matrix.

At the same time, the precipitates located at the boundaries of the grains and subgrains were much larger (Figure 7d). They probably formed during the first step of annealing, i.e., at 300 °C (Figure 6d). The fraction of large precipitates were small enough, compared with nanoparticles located inside subgrains. It should be noted that the size of subgrains do not change significantly, compared to the W300 state (see Figures 6a and 7a). Thus, Zr-containing nanoparticles stabilize the structure upon heating up to 400 °C, which is extremely important for heat resistant conductive alloys [32,33].

As can be seen from Table 2, the experimental alloy has a good combination of strength and electrical conductivity (the UTS and EC are 234 MPa and 55.6 IACS, respectively), meeting the AT2 type specification [1,32]. At the same time, the maximum heating temperature (standard heat resistance test) was much higher, and mechanical properties obtained meet the AT4 type specification. As can be seen from Table 1, the total annealing time was less than 10 h and probably can be further decreased (if to eliminate intermediate steps, see Figure 1). In any case, it is much less than the typical annealing time for CCR wire rods (hundreds of hours).

Table 2. Mechanical and electrical properties of Al–Zr wire alloys.

Alloy	Maximal Temperature of Heating, °C	UTS, MPa	YS, MPa	El, %	ER, nΩm	Conductivity, %IACS
EMC Al–0.6%Zr(Fe,Si)	400	234 ± 5	207 ± 7	6.8 ± 0.7	31.0 ± 0.1	55.6
AT2/KTAL (High-Strength Thermal Resistant Aluminum Alloy)	230	225–248	-	1.5–2.0	31.347	55.0
AT4/XTAl (Extra Thermal Resistant Aluminum Alloy)	400	159–169	-	1.5–2.0	29.726	58.0

The fracture surface of the experimental wire alloy after a tensile test has a homogeneous ductile fine-dimpled pattern (Figure 8a). The size of the dimples is significantly larger than that of iron-bearing particles inside the dimples (Figure 8b). No oxides or nonmetallic inclusions were found. Thus, the EMC technology provides for melt refining, despite high process temperature.

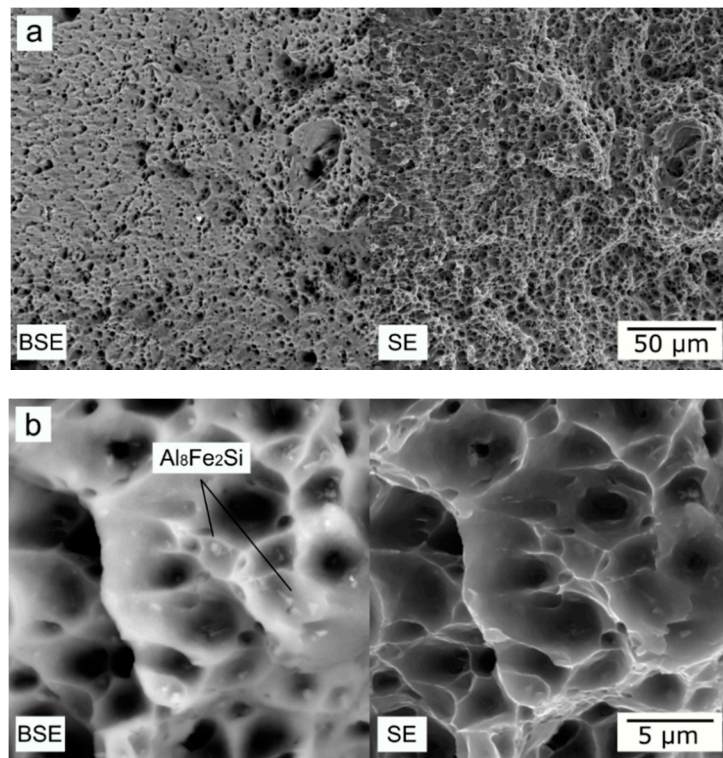


Figure 8. Fracture surfaces of experimental wire alloy (W400 see in Table 1), SEM, **left**—back scattered electron image, **right**—secondary electron image, (a) small magnification, (b) high magnification.

4. Summary

1. The experimental aluminum alloy, containing 0.6%Zr, 0.4%Fe and 0.4%Si (wt.%), was manufactured by the method of electromagnetic casting (EMC) in the form of long-length rod 12 mm in diameter. The as-cast EMC rod has high ductility when cold drawing a wire with a high degree of deformation (94%). High deformability of as-cast rods can be explained by favorable microstructure, e.g., small size of the dendritic cells (about 4 μm), submicron eutectic particles of $\text{Al}_8\text{Fe}_2\text{Si}$ phase, and almost full dissolving of Zr in Al solid solution.
2. The effect of annealing temperature (up to 600 °C) on the hardness and electrical resistivity (ER) of EMC rod, cold rolled strip, and cold drawn wire were studied. It was shown that the temperature dependences of ER for the cold deformed strip and the wire were very close. The best combination of hardness and ER in the cold rolled strip was reached after annealing at 400 °C.
3. TEM study of structure evolution in the as-drawn wire revealed the onset of Al_3Zr (L_{12}) nanoparticle formation at 300 °C, and almost complete decomposition of (Al) at 400 °C. The distribution of the nanoparticles was quite homogeneous, with their average size not exceeding 10 nm. At the same time, the precipitates at subgrain boundaries were much larger. Zr-containing nanoparticles allow one to stabilize the structure upon heating up to 400 °C, which is extremely important for heat resistant conductive alloys.
4. The experimental wire alloy has UTS and EC (234 MPa and 55.6 IACS, respectively) meeting the AT2 type specification. At the same time, the maximum heating temperature was much higher (400 versus 230 °C) and mechanical properties obtained meet the AT4 type specification. The possibility of electromagnetic casting of wire rods suitable for direct cold drawing would be a substantial economic advantage.

Author Contributions: Conceptualization, N.B.; investigation, N.K. and M.M.; methodology, V.T. and T.A.; supervision, N.B.; writing—original draft, N.B.; Writing—review & editing, M.M., T.A., and N.K. All authors have read and agreed to the published version of the manuscript.

Funding: The study was carried out within the framework of the implementation of the Resolution of the Government of the Russian Federation of April 9, 2010 No. 220 (Contract No. 074-02-2018-329 from May 16, 2018).

Acknowledgments: The results were obtained by using the equipment of RPC Magnetic hydrodynamics LLC, Krasnoyarsk, Russia; Institute of Physics of Advanced Materials, Ufa State Aviation Technical University, Ufa, Russia; and Department of metal forming, National University of Science and Technology MISiS, Moscow, Russia.

Conflicts of Interest: The authors declare no conflict of interest.

References

1. ASTM B941-16. *Standard Specification for Heat Resistant Aluminum-Zirconium Alloy Wire for Electrical Purposes*; ASTM International: West Conshohocken, PA, USA, 2016; pp. 1–4.
2. Brubak, J.P.; Eftestol, B.; Ladiszlaidesz, F. Aluminium Alloy, a Method of Making it and an Application of the Alloy. IFI CLAIMS Patent Services. U.S. Patent 5,067,994, 26 November 1991. Available online: <https://patents.google.com/patent/US5067994A/en?q=5067994> (accessed on 20 February 2019).
3. Knych, T.; Jablonsky, M.; Smyrak, B. New aluminium alloys for electrical wires of fine diameter for automotive industry. *Arch. Metall. Mater.* **2009**, *54*, 671–676. Available online: https://www.researchgate.net/publication/263734063_New_aluminium_alloys_for_electrical_wires_of_fine_diameter_for_automotive_industry (accessed on 20 May 2009).
4. Properzi, I. Machine for the Continuous Casting of Metal Rod. IFI CLAIMS Patent Services. U.S. Patent 2,659,948A, 24 November 1953. Available online: <https://patents.google.com/patent/US2659948A/en?q=2659948> (accessed on 25 February 2019).
5. Southwire Company. Available online: <https://www.southwire.com> (accessed on 28 February 2019).
6. Belov, N.A.; Alabin, A.N.; Matveeva, I.A.; Eskin, D.G. Effect of Zr additions and annealing temperature on electrical conductivity and hardness of hot rolled Al sheets. *Trans. Nonferrous Met. Soc. China* **2015**, *25*, 2817–2826. [[CrossRef](#)]
7. Knipling, K.E.; Karnesky, R.A.; Lee, C.P.; Dunand, D.C.; Seidman, D.N. Precipitation evolution in Al–0.1Sc, Al–0.1Zr and Al–0.1Sc–0.1Zr (at.%) alloys during isochronal aging. *Acta Mater.* **2010**, *58*, 5184–5195. [[CrossRef](#)]
8. Deschamp, A.; Guyo, P. In situ small-angle scattering study of the precipitation kinetics in an Al–Zr–Sc alloy. *Acta Mater.* **2007**, *55*, 2775–2783. [[CrossRef](#)]
9. Lefebvre, W.; Danoix, F.; Hallem, H.; Forbord, B.; Bostel, A.; Marthinsen, K. Precipitation kinetic of Al₃(Sc,Zr) dispersoids in aluminium. *J. Alloys Compd.* **2009**, *470*, 107–110. [[CrossRef](#)]
10. Forbord, B.; Lefebvre, W.; Danoix, F.; Hallem, H.; Marthinsen, K. Three dimensional atom probe investigation on the formation of Al₃(Sc,Zr)-dispersoids in aluminium alloys. *Scrip. Mater.* **2004**, *51*, 333–337. [[CrossRef](#)]
11. Clouet, E.; Barbu, A.; Lae, L.; Martin, G. Precipitation kinetics of Al₃Zr and Al₃Sc in aluminum alloys modeled with cluster dynamics. *Acta Mater.* **2005**, *53*, 2313–2325. [[CrossRef](#)]
12. Çadırlı, E.; Tecer, H.; Sahin, M.; Yılmaz, E.; Kırındı, T.; Gündüz, M. Effect of heat treatments on the microhardness and tensile strength of Al–0.25 wt.% Zr alloy. *J. Alloy Compd.* **2015**, *632*, 229–237. [[CrossRef](#)]
13. Robson, J.D.; Prangnell, P.B. Dispersoid precipitation and process modelling in zirconium containing commercial aluminium alloys. *Acta Mater.* **2001**, *49*, 599–613. [[CrossRef](#)]
14. Avdulov, A.A.; Usynina, G.P.; Sergeev, N.V.; Gudkov, I.S. Otlitchitel'nyye osobennosti struktury i svoystv dlinnomernykh slitkov malogo secheniya iz alyuminiyevykh splavov, otlitykh v elektromagnitnyy kristallizator. (Distinctive features of the structure and properties of long ingots of small cross section from aluminum alloys cast in an electromagnetic mold). *Tsvet. Met.* **2017**, *7*, 73–77. [[CrossRef](#)]
15. Dobatkin, V.I.; Elagin, V.I.; Fedorov, V.M. *Bystrozakristallizovannyealyuminieovyeplyavy (Rapidly Solidified Aluminum Alloys)*; VILS: Moscow, Russia, 1995; pp. 43–59.
16. Polmear, I.J. *Light Alloys. From Traditional Alloys to Nanocrystals*, 5th ed.; Butterworth-Heinemann: Oxford, UK, 2006; pp. 129–130.
17. Belov, N.A.; Korotkova, N.O.; Akopyan, T.K.; Timofeev, V.N. Structure and properties of Al–0.6%Zr–0.4%Fe–0.4%Si (wt%) wire alloy manufactured by electromagnetic casting. *JOM* **2020**, *72*, 1561–1570. [[CrossRef](#)]
18. RPC Magnetic Hydrodynamics, LLC. Available online: <http://www.npcmgd.com> (accessed on 25 April 2020).
19. IEC 60468:1974. *Method of Measurement of Resistivity of Metallic Materials*; IEC: Geneva, Switzerland, 1974.

20. Bäckerud, L.; Chai, G.; Tamminen, J. *Solidification Characteristics of Aluminum Alloys. Vol. 1: Foundry Alloys*; Skanaluminium: Oslo, Norway, 1986; pp. 9–26.
21. Glazoff, M.V.; Khvan, A.V.; Zolotarevsky, V.S.; Belov, N.A.; Dinsdale, A.T. *Casting Aluminum Alloys. Their Physical and Mechanical Metallurgy*; Elsevier: Oxford, UK, 2019; pp. 180–186.
22. Belov, N.A.; Aksenov, A.A.; Eskin, D.G. *Iron in Aluminum Alloys: Impurity and Alloying Element*; Fransi and Tailor: London, UK, 2002; pp. 43–68.
23. Belov, N.A.; Eskin, D.G.; Aksenov, A.A. *Multicomponent Phase Diagrams: Applications for Commercial Aluminum Alloys*; Elsevier: Amsterdam, The Netherlands, 2005; pp. 19–31.
24. Gao, T.; Ceguerra, A.; Breen, A.; Liu, X.; Wu, Y.; Ringer, S. Precipitation behaviors of cubic and tetragonal Zr-rich phase in Al-(Si)-Zr alloys. *J. Alloys Compd.* **2016**, *674*, 125–130. [[CrossRef](#)]
25. Yea, J.; Guana, R.; Zhao, H.; Yinc, A. Effect of Zr content on the precipitation and dynamic softening behavior in Al-Fe-Zr alloys. *Mater. Charact.* **2020**, *162*, 110–181. [[CrossRef](#)]
26. Vlach, M.; Stulíková, I.; Smola, B.; Žaludová, N.; Černá, J. Phase transformations in isochronally annealed mould-cast and cold-rolled Al-Sc-Zr-based alloy. *J. Alloy Compd.* **2010**, *492*, 143–148. [[CrossRef](#)]
27. Belov, N.A.; Korotkova, N.O.; Alabin, A.N.; Mishurov, S.S. Influence of a silicon additive on resistivity and hardness of the Al-1% Fe-0.3% Zr alloy. *Russ. J. Non-Ferrous Metals* **2018**, *59*, 276–283. [[CrossRef](#)]
28. Jiang, J.; Jiang, F.; Zhang, M.; Tang, Z.; Tonga, M. Recrystallization behavior of Al-Mg-Mn-Sc-Zr alloy based on two different deformation ways. *Mater. Lett.* **2020**, *265*, 127455. [[CrossRef](#)]
29. Fu, J.; Yang, Z.; Deng, Y.; Wu, Y.; Lu, J. Influence of Zr addition on precipitation evolution and performance of AlMg-Si alloy conductor. *Mater. Charact.* **2020**, *159*, 110021. [[CrossRef](#)]
30. Zhang, J.; Wang, H.; Yia, D.; Wanga, B.; Wang, H. Comparative study of Sc and Er addition on microstructure, mechanical properties, and electrical conductivity of Al-0.2Zr-based alloy cables. *Mater. Charact.* **2018**, *145*, 126–134. [[CrossRef](#)]
31. Vlach, M.; Stulíková, I.; Smola, B.; Piesova, J.; Cisarova, H.; Danis, S.; Plasek, J.; Gemma, R.; Tanprayoon, D.; Neuber, V. Effect of cold rolling on precipitation processes in Al-Mn-Sc-Zr alloy. *Mat. Sci. Eng. A* **2012**, *548*, 27–32. [[CrossRef](#)]
32. Knych, T.; Piwowska, M.; Uliasz, P. Studies on the process of heat treatment of conductive AlZr alloys obtained in various productive processes. *Arch. Metal. Mater.* **2011**, *56*, 687–692. [[CrossRef](#)]
33. Orlova, T.S.; Mavlyutov, A.M.; Latynina, T.A.; Ubyivovk, E.V.; Murashkin, M.Y.; Schneider, R.; Gerthsen, D.; Valiev, R.Z. Influence of severe plastic deformation on microstructure strength and electrical conductivity of aged Al-0.4Zr (wt.%) alloy. *Rev. Adv. Mater. Sci.* **2018**, *55*, 92–101. [[CrossRef](#)]



© 2020 by the authors. Licensee MDPI, Basel, Switzerland. This article is an open access article distributed under the terms and conditions of the Creative Commons Attribution (CC BY) license (<http://creativecommons.org/licenses/by/4.0/>).